Modeling the receptivity of an air jet to transverse acoustic disturbance with application to musical instruments

F. Blanc
UME-ENSTA-ParisTech, Chemin de la Hunière, F-91761 Palaiseau Cedex, France

V. François and B. Fabre
Sorbonne Universités, UPMC Univ Paris 06, UMR 7190, Institut Jean le Rond d'Alembert, LAM, Paris, France

P. de la Cuadra
Pontificia Universidad Católica de Chile, CITA, Jaime Guzman 3300, Santiago, Chile

P.-Y. Lagrée
Sorbonne Universités, UPMC Univ Paris 06, UMR 7190, Institut Jean le Rond d'Alembert, LAM, Paris, France

(Received 7 November 2013; accepted 10 April 2014)

A simple analytical model for the interaction between a plane jet issued from a flue and a transverse acoustic disturbance is developed in this paper. The model is inspired by direct flow simulation results confronted to experimental data. The interaction is expected to take place in the vicinity of the separation points of the jet. The influence of the detailed geometry of the channel end on the jet receptivity is discussed, and more specifically the chamfer geometries found in flute-like musical instruments. The simplified model explains quite well the difference between the jet response of a flue with square edges compared to a chamfered flue exit. The effect of rounded, lip-like flue exit is not well captured by the model.
 [http://dx.doi.org/10.1121/1.4874598]

PACS number(s): 43.28.Gq [AH] Pages: 3221–3230

I. INTRODUCTION

Jets are known to be unstable systems, that amplify any small perturbation, depending on its frequency (Drazin[1]). Jet instabilities play an important role in various processes such as atomization in an engine, flow noise, and flue musical instruments. The instability mechanism relies on the concentration of the vorticity in the shear layers of the jet. While the description of jet instability has been widely discussed in the literature, the question of the triggering and the forcing of the instability by an acoustic disturbance is seldom addressed. This paper deals with the so called receptivity of a jet, that links up the jet displacement to an external disturbance.

The temporal instability of an infinite jet has been described by Rayleigh,[2] in the frame-work of a two-dimensional linear inviscid incompressible flow description. In his description, harmonic perturbations of the flow at a given wave number K grow exponentially in time, while convected downstream along the flow.

In Rayleigh's description, the frequency dependence of the instability is determined by the jet velocity profile. Jet instability presents a maximum at a given frequency, depending on the jet and shear layers width, and on the jet velocity. Though Rayleigh's description exhibits a complexity that requires numerical computation for non-trivial velocity profiles, it relies on assumptions (inviscid, incompressible, linear) that are seldom met in most applications where jet instabilities occur.

The case of viscous jets is described with the Orr–Sommerfeld equations. With this model, the jet instability is affected by the Reynolds number of the flow. It is also noteworthy that some stable solutions of the Rayleigh equation prove to be unstable with the Orr–Sommerfeld model (Drazin and Howard[3]).

Moreover, the linear description of the perturbations' evolution is only valid for small transversal displacements of the jet compared to its width. Depending on the amplitude of the perturbation the jet breaks down into a discrete vortex street at a certain distance from the flue (Meissner[4]). Holger,[5] without analyzing in details this transformation process, relates the properties of the vortex street with those of the jet for an edge tone configuration. In the case of one shear layer interacting with an acoustic field Dequand,[6] combines the model of Holger[5] with the model of Nelson[7] to describe the limit cycle of the oscillation of the jet in flue instruments. Each vortex shedding is created at a particular phase of the periodic acoustic field. Its strength and convection velocity depends on the velocity of the flow.

In many systems the jet emerges from an opening called the *flue*, and is submitted to the disturbances at its birth. In such configurations, one cannot describe the flow as an infinite jet. The jet is divided into three regions: the flue, where the perturbations are triggered, the linear region, where these perturbations grow, and the vortex street, where the perturbations are sufficiently large to form individual vortices that convect downstream. Our study will be restricted to the first two regions. In particular, one has to initiate the displacement of the jet at the flue. The relation between the transverse disturbance and the initial jet displacement is known as the receptivity of the jet. The present paper discusses the receptivity of a laminar planar jet with an emphasis on flue musical instruments.

Different models of jet receptivity can be found in the literature: According to Fletcher,[8] the initial hydrodynamic displacement of the jet at the flue exit is the result of its opposition to the acoustic displacement. Fletcher[8] argues that the jet transversal displacement is the sum of the hydrodynamic and acoustic displacements. He assumes that this initial displacement should vanish. Verge,[9] including the acoustic velocity in the Kutta condition at the jet separation points, describes the effect of the acoustic field as a modulation of the vorticity in the shear layers of the jet. More recently, Ségoufin[10] proposes to include the acoustic disturbance as a velocity correction in the Rayleigh's equation.

Another approach is given by de la Cuadra *et al.*,[11] who propose an empirical model based on jet visualizations. In this experiment, that will be discussed in Sec. II, the initial displacement is estimated from the displacement of the jet far from the flue.

All of the models described above do not consider the geometry of the exit of the formation flue. But, according to recorder makers (Ségoufin[12] and Blanc[13]), this geometry is of crucial importance for the proper dynamical behavior of the instruments as well as to produce a good tone quality. Therefore, it is of great importance to develop a model that includes the effect of the channel the geometry of the exit of the flue channel. Ségoufin[12] studied the effects of modifications of the geometry on the oscillating behavior of an experimental recorder. Her study related the channel exit geometry with changes on the regimes stability and on the transient behavior of the instrument.

A preliminary study (Blanc *et al.*[13,14]) showed that the exit geometry has a very small impact on the birth of the unperturbated jet, and especially on the location of the separation points, where the flow leaves the channel walls. Thus, the geometry is expected to affect mainly the receptivity of the jet.

In this paper, we aim at developing the simplest model of the receptivity of a jet to transverse acoustic disturbances, that takes into account the geometry of the flue. This work is based on experimental jet visualizations and develops a very simple analytical model.

After a presentation of the experimental setup (Sec. II), the hypotheses and equations of the model—the core of this paper—are presented (Sec. IV), followed by the predictions of the model and comparison with the experimental results.

II. SETUP OF EXPERIMENTS

The basic setup consists of a jet, which without any external disturbances would create a velocity field $U_0(y)$ in the x-direction, function of the transverse coordinate y. The jet is submitted to a harmonically oscillating velocity field with the pulsation ω, which without the jet would be $[u_w(x, y, t), v_w(x, y, t)]$. The interaction between both flows creates a perturbed jet $\vec{U}(x, y, t)$. The setup allows one to change the geometry of the flue.

Three channel exit geometries are used: an exit with rectangular edges (squared exit), a 45-deg-chamfered exit, and a rounded exit, shown in Fig. 1. The choice of these geometries is guided by their use in flutes such as organ pipes, recorders, and human lips for the transverse flute. The origin of the abscissa axis is set in the place where the parallelepipedic channel ends and the exit shape begins, as shown in Fig. 1.

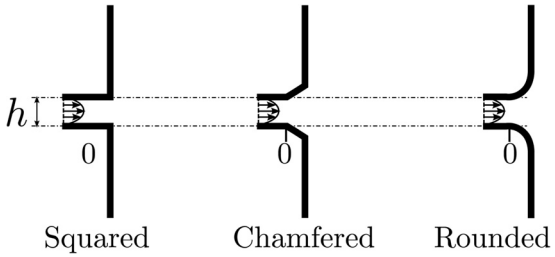

FIG. 1. The three channel exit geometries studied.

de la Cuadra[11] developed an experimental setup that allows one to focus on the interaction between the acoustic field and the jet. In his setup, the jet is created by raising the pressure in a cavity connected to a flue channel with a specific flue geometry and emerges from this artificial mouth into the open air. The disturbances are created by loudspeakers to allow full control of their amplitude and frequency. With this setup, we can use the same blowing and disturbance conditions for the different flue geometries. As the experimental device has a width $H = 20h$, the jet is supposed to be two-dimensional.

The experimental setup, detailed by de la Cuadra,[11] is presented in Sec. 1 of the Appendix. The jet is visualized and detected via image processing for different phases of its oscillation.

Figure 2 presents a typical image of the jet visualizations. It can be seen that the jet presents an oscillation growing along its path, and resulting in the formation of vortices. Further downstream, the flow presents a turbulent behavior.

III. AMPLIFICATION OF A PERTURBATION TO THE JET

The harmonic perturbation of the jet results into an oscillating motion of the jet, which amplifies as it is convected downstream. The position of the jet in the successive images from flow visualization is detected using automatic image analysis, as proposed by de la Cuadra *et al.*[11]

The amplitude and the phase of the oscillation of the jet at the frequency of the disturbance are then extracted by digital Fourier transform at every distance from the mouth. This way, the displacement amplitude (and phase) versus the distance from the mouth is estimated.

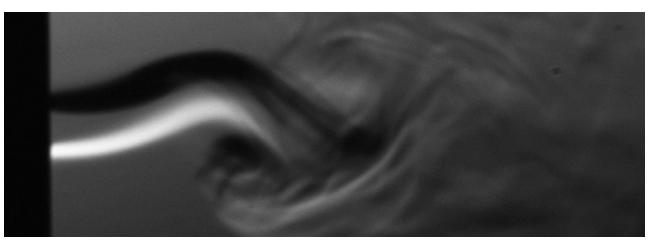

FIG. 2. Typical image of the jet in the experiments ($\mathrm{Re} = 500$ and $\mathrm{St} = 0.37$).

As in the paper of de la Cuadra *et al.*,[11] the flow visualizations are analyzed within the framework of Rayleigh's description for an inviscid two-dimensional flow. Rayleigh's theory has been widely used as a framework in the study and modeling of unstable jets (Verge,[9] Fletcher,[8,15] Nolle,[16] Mattingly and Criminale[17]) and is described in the next section.

We follow here the classical spatial linear instability theory of a basic jet flow $U_0(y)$. The linear perturbation stream function ψ is of the form (Rayleigh,[2] Mattingly and Criminale,[17] de la Cuadra[18]) $\psi(x, y, t) = \Re\,[\phi(y)e^{i(Kx-\omega t)}]$.

The jet instability is expressed by the fact that either K—if the instability is studied space wise—or ω—if the instability is studied time wise—has an imaginary part resulting in an exponential increase or decrease of the perturbation. In de la Cuadra's experiments, because the oscillation frequency is imposed, ω is real while K is complex and satisfies Rayleigh's equation:

$$\left(U(y) - \frac{\omega}{K}\right)\left(\frac{\partial^2\phi}{\partial y^2} - K^2\phi\right) - \frac{\partial^2 U(y)}{\partial y^2}\phi = 0. \tag{1}$$

This equation relies on the hypothesis that $\mathrm{Re} \gg 1$ and $\partial U_0/\partial x$ is negligible. It assumes also that the jet is infinitely long.

The dispersion relation $K(\omega)$ gives the amplification and the phase velocity of the perturbation stream function as a function of the jet velocity profile.

In the case of an infinite Bickley jet velocity profile, the numerical resolution of Eq. (1) has been carried out by Mattingly and Criminale.[17]

Rayleigh's theory predicts a jet stream function ϕ, while in the experiments as in the simulations, only the jet transverse displacement η is observed. The jet being a streakline, in order to compute η, one should in principles compute

$$\eta(x,t) = \int_{t-x/Uj}^{t} \frac{\partial\phi[x-(t-t')U]}{\partial x} dt', \tag{2}$$

where U_j is the maximum of the velocity profile of the jet.

The relation between ϕ and η is complex and will not be used. Different simplified models exist (Verge,[19] de la Cuadra,[18] Fletcher[8,15]).

For the sake of simplicity, the jet transverse displacement detected at the disturbance frequency is fitted to the model of jet displacement η proposed by de la Cuadra:[11]

$$\eta(x,t) = \Re\left(\eta_0 e^{\alpha x} e^{i(\mathrm{kx}-\omega \mathrm{t})}\right), \tag{3}$$

as an exponentially amplifying wave. The phase of the displacement is related to the velocity of the wave $c = \omega/k$, and its amplitude is described by the parameter $\eta_0 e^{\alpha x}$, and is thus assumed to grow exponentially with the distance from the mouth. The amplitude of the jet displacement versus the distance from the mouth is fitted by an exponential function in order to estimate α and η_0. Figure 3 presents the dimensionless amplification coefficient αh as function of the Strouhal number $\mathrm{St} = \omega h/U_0$ for the three different flue exit geometries used in the present study, as obtained through image analysis.[11]

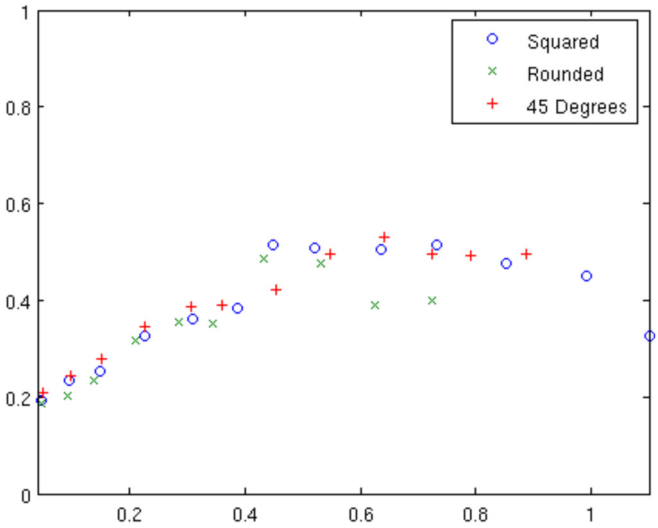

FIG. 3. (Color online) Amplification coefficient of the jet αh as function of the Strouhal number $\mathrm{St} = \omega h/U_0$ for three different flue exit geometries, at $\mathrm{Re} = 200$. From Ref. 7.

IV. THE MODEL

The receptivity model presented in this paper has been developed with two aims: On the one hand, it has to take into account the geometry of the flue and on the other hand, we want to keep it as simple as possible.

Because of viscosity, the velocity vanishes at the walls. The initial perturbation of the jet by the transverse velocity field is expected to be localized at the position where the main flow separates from the wall, resulting in a jet convecting a modulation of the vorticity of its shear layers. Therefore, a model of the receptivity should consider the details of the velocity field around the jet formation points, at distances on the order of the boundary layers thickness. Please note that two boundary layers are to be considered: A stationary flow boundary layer, resulting from the action of viscosity along the jet flue and an acoustic boundary layer, resulting from the action of viscosity along the wall due to the oscillating acoustic flow.

The flow simulations presented in Sec. 2 of the Appendix (Blanc *et al.*[20]) suggest a way to describe the initial jet perturbation in different flue exit geometries. The details of the velocity field (Fig. 4) show two effects of the geometry near the separation points: First, the depth of the geometry protects the flue exit from the disturbance; second, the shape of the geometry determines the angle of the disturbing field in the vicinity of the jet formation points, where the initial jet perturbation is expected to take place.

In this very simple model, we will first only take into account the orientation effect: The angle of the disturbance is expressed by decomposing the perturbation into a longitudinal component, u_w and a transverse component, v_w, which are equal to the disturbance components.

To solve the receptivity problem it is necessary to compute the basic flow and the disturbance separately. This

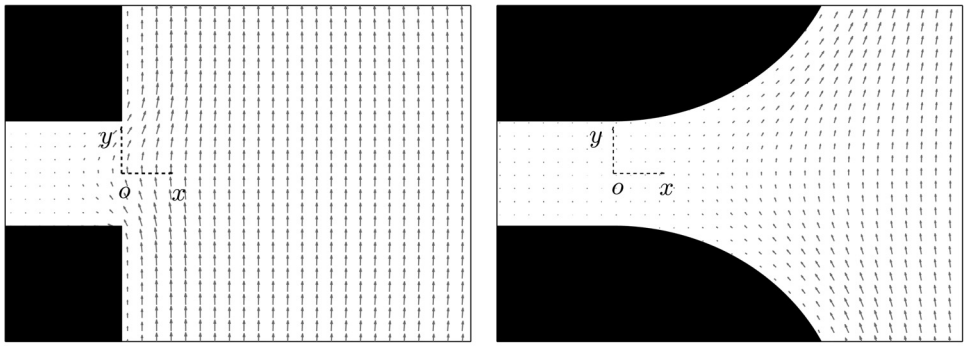

(a) (b)

FIG. 4. Perturbation fields simulated for two different geometries (from Ref. 6). The geometry of the mouth gives to the perturbation its orientation and protects the flue from direct perturbations.

could be done numerically with the main problem being to overcome the intrinsic instability of the jet.

Here, an analytical approach, that implies a further simplification of the problem, is chosen. The purpose of the model is to predict the initial displacement of a jet emerging from a given flue geometry and submitted to a transverse disturbance.

A. Assumptions of the receptivity model

The assumptions used in our theoretical model are presented in this section. The transverse acoustic field is considered as a perturbation velocity on a basic flow. The exit geometry affects the orientation of the perturbating velocity.

The flow in the channel is assumed to be a fully developed Poiseuille flow (Tritton[21]). Moreover the jet is supposed not to spread. In particular we assume the conservation of the velocity profile of the flow inside the channel: the velocity $U(y)$ of the jet has the form of a Poiseuille flow for $|y| \leq h/2$ and it vanishes $U(y) = 0$ for $|y| \geq h/2$. As shown in Sec. IV B, this assumption concerning $U(y)$ has only a small effect on the instability of the jet for low Strouhal numbers, and simplifies the flow at the separation points.

Hence, we consider that the unperturbated flow is simply an infinite Poiseuille flow, unaffected by the separation at the flue. The next step of simplification is then to consider that the perturbation due to the acoustic field occurs all along the flow. This last assumption means that the spatial geometry variations, such as the height of the channel are very slow compared to the spatial variations of the velocity profile. Assuming the perturbations occurring all along the infinite Poiseuille flow ensure to have a translation invariant system. This is a very efficient simplification of the problem, as it suppresses the convection terms in the flow direction, allowing an analytical solution.

With these assumptions, one cannot expect to describe known jet behaviors such as its spreading. Moreover, considering a translation invariant flow is in contradiction with the fact that the disturbance has only an influence close to the separation points of the jet (Verge[9]) For a given acoustical perturbation at the separation point $x = 0$, our receptivity model will provide us with an estimate of the perturbed jet velocity profile at $x = 0$. This will be used as an input for an inviscid perturbation model based on Eq. (1).

The system considered in our model is sketched in Fig. 5.

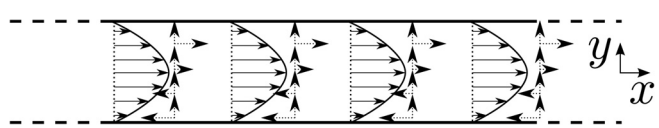

FIG. 5. Schematics of the system considered in the model. Both the base velocity profile (full line) and the perturbation velocity (dashed arrows) are translation invariant in the x-direction.

B. Influence of the jet velocity profile on its instability

Before presenting the model, the next section discusses the influence of the jet velocity profile on its instability. Jets are known[1] to spread and to present velocity profiles that exhibit inflection points. In order to quantify the error due to the Poiseuille-jet hypothesis, the Rayleigh instability Eq. (1) is integrated for three different velocity profiles: a Bickley, a top hat and a Poiseuille. All jets share the same central (maximum) velocity and total mass flux.

Figure 6 shows that the instability of the different velocity profiles present quite similar dependency with the Strouhal number $\mathrm{Str}_h = \omega \mathrm{h}/Uj$, where ω is the pulsation, U_j the maximum of the jet velocity profile, and h is the width of the jet. At $\mathrm{Str}_h = 0.4$ the variation of $K_i h$ for top-hat profile and for Bickley profile are on the order of magnitude of about 15% as compared to the Poiseuille profile. For larger Str_h the curve exhibits a behavior depending on the details of the jet profile. Please note that the maximum value of Str_h under normal oscillation in flute-like musical instruments in

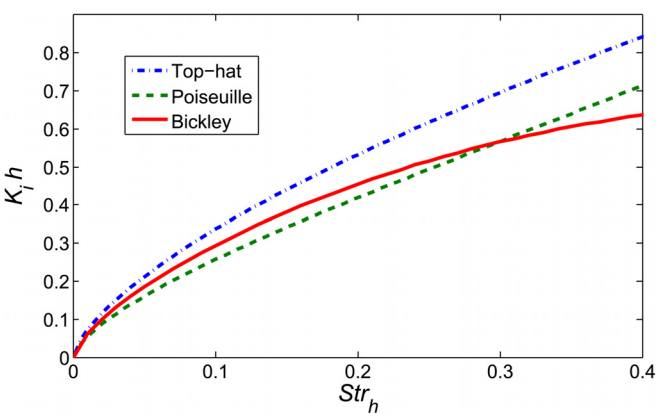

FIG. 6. (Color online) Imaginary part of the complex wave number K_i, as calculated from numerical integration of Rayleigh's equation for different velocity profiles. The different velocity profiles share the same central (maximum) jet velocity and volume flux.

the experiments reported by Verge[22] is 0.17 while the experimental data reported by Auvray[23] show Str_h maximum value of 0.32.

Thus, considering a Poiseuille velocity profile in the jet is not expected to have a dramatic effect on the prediction of its instability, in the range of Strouhal numbers typical for flute-like instruments.

C. Equations of the model

Since the amplitude of the acoustical perturbation is small compared to the main flow velocity ($v_{ac}/U_0 \ll 1$), only first order approximations are considered. The flow is described as incompressible, because $U_0 \ll c_0$, where c_0 is the sound speed and $h \ll \lambda$, where $\lambda = 2\pi c_0/\omega$ is the acoustic wavelength. The acoustical perturbation is split into two contributions: u_w and v_w, parallel and normal to the flow direction. The perturbation of the flow results in a velocity correction $\tilde{u}$ and $\tilde{v}$ to the Poiseuille velocity profile.

Far from the flue, the acoustical perturbation is assumed to be purely transverse (i.e., in the y direction). Near the flue, considering an inviscid fluid description, we assume that the acoustical perturbation field follows the flue geometry. Figure 4 suggests that in the height of the channel, v_w is constant and u_w varies linearly.

Thus, we write

$$\begin{cases} \overline{u_w} = -2\overline{u_{w0}}\bar{y}, \\ \overline{v_w} = \overline{v_{w0}}, \\ |\bar{y}| \le \dfrac{1}{2}. \end{cases} \tag{4}$$

In Eq. (4), u_{w0} and v_{w0} are given by the orientation of the perturbation. Here, we consider three geometries: a squared one, a chamfered one, and a rounded one. As a caricature inspired by the simulations presented Fig. 4, we consider the perturbation in the vicinity of the main flow separation points to be dominated by its transverse component ($u_{w0} = 0$) in the case of a squared outlet, to be equal in both directions ($u_{w0} = v_{w0}$) in the case of a chamfered outlet and to be dominated by its longitudinal component ($v_{w0} = 0$) in the case of a rounded outlet.

In the following, we consider dimensionless quantities, that are written with an overline. Velocities are related to the center velocity of the Poiseuille flow $U_j = U_0(0)$ $(u_w, v_w) = (\overline{u_w}, \overline{v_w}) \times U_j$, and lengths are related to the channel height $h(y = \bar{y}h)$, while the time $t = \bar{t}(h/U_j)$. The velocity field is described by Eq. (5), where St is the dimensionless angular frequency:

$$\begin{cases} \bar{U}_0(\bar{y}) = -4\left(\bar{y}^2 - \dfrac{1}{4}\right), \\ \bar{U} = \bar{U}_0(\bar{y}) + [\tilde{u}(\bar{y}) + \overline{u_w}]e^{iS\bar{t}\bar{t}}, \\ \bar{V} = 0 + [\tilde{v}(\bar{y}) + \overline{v_w}]e^{iS\bar{t}\bar{t}}. \end{cases} \tag{5}$$

The incompressibility equation $\partial\bar{U}/\partial\bar{x} + \partial\bar{V}/\partial\bar{y} = 0$ leads to $\partial\tilde{u}/\partial\bar{x} + \partial\tilde{v}/\partial\bar{y} = 0$. As the system is translation invariant, we have $\partial\tilde{v}/\partial\bar{y} = 0$. Considering the no penetration condition at the upper and lower boundaries of the channel, this means simply that $\tilde{v} = 0$: The correction is parallel to the basic flow.

The projection of the dimensionless inviscid Navier-Stokes equation on the x axis is written in Eq. (6):

$$\frac{\partial\bar{U}}{\partial\bar{t}} + \bar{U}\frac{\partial\bar{U}}{\partial\bar{x}} + \bar{V}\frac{\partial\bar{U}}{\partial\bar{y}} = -\frac{\partial\bar{P}}{\partial\bar{x}}. \tag{6}$$

Using the first equation in Eq. (5), Eq. (6) can be simplified. Considering the remaining terms and neglecting the second order terms in the perturbations leads to a partial differential equation [Eq. (7)]:

$$i\,St\tilde{u} + \overline{v_{w_0}}\frac{\partial\tilde{u}}{\partial y} = 2(\overline{u_{w_0}} + 4\overline{v_{w_0}})y - 2\overline{u_{w_0}}\,\overline{v_{w_0}}. \tag{7}$$

For small amplitude of perturbation, we only consider first order terms. This leads to

$$\tilde{u} = \frac{2i}{St}(\overline{u_{w_0}} + 4\overline{v_{w_0}})\bar{y}. \tag{8}$$

The solution $\tilde{u}$ in Eq. (8) depends on several parameters. The amplitude of the perturbating velocity depends directly on the existence of chamfers that protect the channel exit from the disturbance field. In the description above, the protection effect is not taken into account and we focus on the influence of the orientation of the perturbation flow in the vicinity of the main flow separation points.

The ratio u_{w0}/v_{w0} expresses the dependence of the correction on the geometry: The shape of the channel exit imposes an orientation to the disturbance field. The more the perturbation velocity (u_{w0}, v_{w0}) is oriented in the flow direction [with a rounded exit for instance ($v_{w0} = 0$)], the greater is the ratio u_{w0}/v_{w0}.

Substituting Eq. (8) in $\bar{U}$ as defined by Eq. (5), we get

$$\bar{U} = -4\left(\bar{y}^2 - \frac{1}{4}\right) + \left[2\overline{u_{w0}}\bar{y} - \frac{2i}{St}(\overline{u_{w0}} + 4\overline{v_{w0}})\bar{y}\right]e^{iS\bar{t}\bar{t}}. \tag{9}$$

Note that as $\tilde{u}$ is a complex quantity and is modulated by $e^{iS\bar{t}\bar{t}}$. It also appears that the oscillating component of the resulting flow velocity has different phases along the transverse direction y of the jet.

D. Discussion: Calculation of the initial displacement

Using Eq. (5), the velocity field in the channel can be rebuilt. The initial Poiseuille velocity profile is distorted, the amount of distortion depending on the phase of the perturbation.

We then define a dimensionless initial transverse displacement of the flow $\bar{\epsilon}_0 = \epsilon_0/h$ depending on the flow distortion. Here $\bar{\epsilon}_0$ is defined as the ordina splitting the velocity profile in two parts of equal volume flow. This is written as

$$\int_{-1/2}^{\bar{\epsilon}_0} \bar{U}\,d\bar{y} = \frac{1}{2}\int_{-1/2}^{1/2} \bar{U}\,d\bar{y}. \tag{10}$$

Solving Eq. (10) for $\bar{U}$ given in Eq. (9), the initial transverse displacement $\bar{\epsilon}_0$ appears as the root of a third order polynomia:

$$-\frac{4}{3}\bar{\epsilon}_0^3-\left(\left[\frac{i}{St}(\overline{u_{w_0}}+4\overline{v_{w0}})-\overline{u_{w0}}\right]e^{iSt\bar{t}}\right)\bar{\epsilon}^2+\bar{\epsilon}_0-\frac{1}{2}\left[\frac{i}{St}(\overline{u_{w0}}+4\overline{v_{w0}})-\overline{u_{w0}}\right]e^{iSt\bar{t}}=0. \quad (11)$$

Considering only the first order terms in $\bar{\epsilon}_0$, we get

$$\bar{\epsilon}_0=\frac{1}{2}\left[\frac{i}{St}(\overline{u_{w_0}}+4\overline{v_{w0}})-\overline{u_{w0}}\right]e^{iSt\bar{t}}. \quad (12)$$

As the perturbation is inviscid, we assume that its direction follows the geometry of the flue at the flow separation points, that is

$u_{w0}=0$ for the squared geometry,
$u_{w0}=v_{w0}$ for the chamfered geometry,
$v_{w0}=0$ for the rounded geometry.

The relation between the perturbation velocities u_{w0}, v_{w0} and the acoustic velocity v_{ac} is not straightforward. Apart from the orientation of the perturbation discussed in the previous section, the flue exit geometry affects the amplitude of the perturbation as well. Indeed, the geometry acts as a protection of the flow separation points from the perturbation generated by the acoustic field. This protection is of course the strongest for the rounded exit and the weakest in the case of a squared exit, the case of the chamfered exit lying in between. In order to quantify the relative protection effect, results from flow simulation in the three different cases are compared.

In Fig. 7 we plot the amplitude of the perturbation versus the abscissa x, taken at the middle height of the mouth in the simulations and with the three geometries studied: The disturbing field is not homogeneous. The amplitude decreases when moving away from the mouth. This is due to the fact that the disturbance is created by velocity boundary conditions on both sides of the mouth, over a small distance relative to the simulation domain length.

Figure 7 shows the protection effect of the mouth geometry: The flue is positioned at $x=0$. At this position, the amplitude of the perturbation is not the same for the three geometries, the squared one appearing to be the less protected, and the rounded one the more protected.

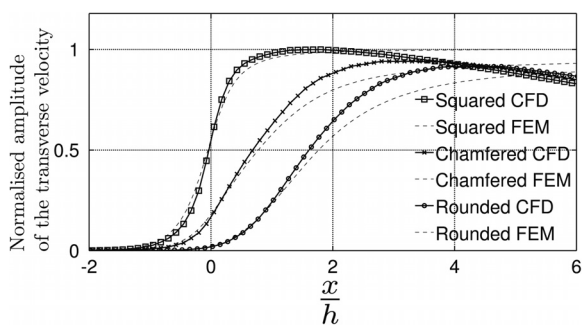

FIG. 7. Amplitude of the transverse component v_w of the disturbing field at half the height of the channel for the three geometries studied. The disturbance velocities are normalized by the jet velocity. The channel exit is at $x=0$. The dotted lines present the modulus of the disturbance resulting from a potential flow computation.

If we define v_{ac} as the maximum of the perturbation amplitude, the estimation of v_w at $x=0$ gives, respectively, the values of the protection factor α for the squared, the chamfered and the rounded geometry $\beta=v_{w0}/v_{ac}=0.6$, $\beta=v_{w0}/v_{ac}=0.2$, and $\beta=v_{w0}/v_{ac}=0.02$. It is important to note that only v_w is displayed in Fig. 7.

The modulus of the transverse component of the disturbance with a potential flow (computed with FreeFem++[24]) is also represented in Fig. 7. Defining ψ as the stream function, the problem solved is $\nabla^2\psi=0$. The boundary conditions are $\psi=0$ on the solid boundaries, $\psi=-V_0x$ on the top and the bottom of the domain, and $\partial\psi/\partial x=-V_0$ far from the channel exit. Close to $x=0$, the results are remarkably in good agreement.

This agreement means that for low disturbance velocities, a potential flow description allows a fairly good prediction of the perturbation field. This is important, as it means that an accurate analytical description of the perturbation taking into account the protection effect can be carried by means of a conformal mapping.[25]

Taking into account the orientation of the perturbating flow as discussed above together with the protection factor β allows to plot the initial jet perturbation as function of the Strouhal number in Fig. 8. For comparison purpose, we assume that $\sqrt{(u_w^2+v_w^2)}=\beta v_{ac}$. The dimensionless initial displacement of the jet $(\epsilon_0U_j)/(v_{ac}h)$ predicted by the model is compared to the experimental value η_0 from de la Cuadra[18] presented in the dimensionless form of $(\eta_0U_j)/(v_{ac}h)$. The initial jet displacement in the experimental analysis by de la Cuadra is estimated from flow visualizations, as discussed in Sec. III. Since this displacement cannot be measured at the flue exit, the values of η_0 are estimated as the amplitude of the exponential function fitted to the data further downstream (Ref. 11). The two definitions of the initial jet displacement are therefore slightly different.

Figure 8 compares the prediction of the model to the experimental results taken from de la Cuadra.[18] For the squared and chamfered geometries, the model offers a fairly good estimation of the jet receptivity, while the prediction for the rounded geometry is one order of

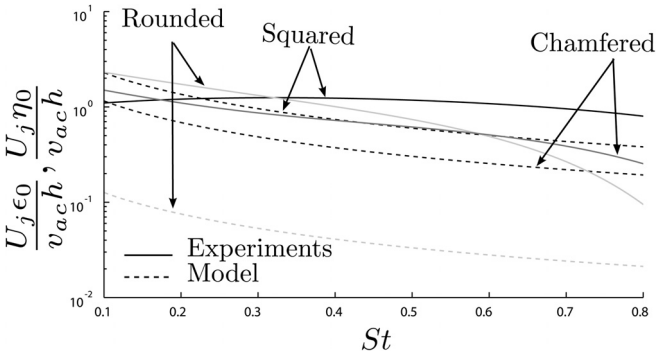

FIG. 8. Comparison of $\epsilon_0U_j/v_{ac}h$ predicted by the model and the experimental data $\eta_0U_j/v_{ac}h$ taken from de la Cuadra, see Ref. 7.

magnitude wrong compared to the experimental values. The low Strouhal number behavior of the velocity correction $\tilde{u}$ predicted shows the effect of the term i/St in Eq. (8). This shows the contribution of the convective terms in Eq. (6), which is therefore expected to vanish at high frequencies.

In spite these drawbacks, the model is able to predict differences in the initial displacement of the jet, due to the shape of the mouth. For $\mathrm{St} \geq 0.6$, these differences are qualitatively in good agreement with the experiments for the squared and chamfered geometries.

V. CONCLUSION

The aim of the paper is to develop a simple model that can take into account the influence of the geometry at the flue exit.

The main idea in the model is to decompose the perturbation field in its longitudinal and transversal components at the expected jet formation points. The ratio of these components, as well as their amplitudes relative to the perturbation is changing according to the geometry at the flue exit. Thus, the effect of the flue exit geometry is modeled as an orientation of the perturbation and a protection from the perturbation of the jet separation points.

The predictions of the model are compared to the experimental values estimated by de la Cuadra.[18] The comparison indicates that in absence of the protection factor, the model overestimates the jet receptivity but presents a reasonable order of magnitude.

Numerical simulations, such as that presented by Blanc,[20] can be used to estimate the protection effect.

Moreover, the frequency behavior in the experiment and the model are different. This may be related to the fact that the translation invariance in the model leads to neglect convection effects. This could be improved, as the disturbance is supposed to take place almost punctually on the jet.

Studying a looped oscillator including the model presented in this paper exhibits a behavior that can be linked to the behavior of recorders with different flue geometries (Blanc[13]). In spite of its simplicity, the model presented allows qualitative prediction of the effects of changing the channel exit geometry, and might be used for real-time simulation of the instrument.

ACKNOWLEDGMENTS

The authors thank André Almeida for the scientific discussions and the support from ECOS-CONICYT and FONDECYT 11090142.

APPENDIX: EXPERIMENTAL MEASUREMENTS AND SIMULATIONS

The following describes the experimental and numerical configurations, and the parameters used to adjust the simulation parameters to the experiments.

1. Experimental setup

The experimental setup used has been described by de la Cuadra[11] and is represented in Fig. 9. CO_2 (viscosity $\nu = 8.04 \times 10^{-6}$ m^2 s^{-1}) is supplied by a 50 bar reservoir through a regulator and feeds the artificial mouth. The flow is controlled by a mass flow regulator (Brooks 5851S). The artificial mouth is a parallelepipedic volume. One of the faces of the mouth is removable and supports the formation channel. Different channel faces are used, according to the three flue geometries studied. The channels dimensions are height $h = 1$ mm, 20 mm wide, and 18 mm long, and the inner volume of the mouth is $5 \times 3 \times 3.5$ cm^3. The scales are chosen so that the large width of the mouth, compared to the channel height favors a two dimensional jet behavior. The typical jet flow is 7.6×10^{-5} m^3 s^{-1}. Assuming a top hat velocity profile, this leads to a jet center velocity of $U_0 = 3.8$ m s^{-1}.

The jet emerging from the mouth is submitted to a transverse velocity field created by two loudspeakers (15 cm in diameter) in phase opposition in order to create a homogenous velocity perturbation together with minimal pressure variations. The experiment is carried for different perturbation frequencies f in the range of $42\,\mathrm{Hz} < f < 322\,\mathrm{Hz}$. The flue is midway of the two loudspeakers and aligned with their centers. The acoustic velocity is measured with a microphone doublet.

Schlieren technique (Merzkirch[26]) is used to visualize the transparent jet. A stroboscope is used in order to light the jet at different oscillation phases. The loudspeakers sine wave excitation and the stroboscope triggering are generated with a TT*i* TGA1244 arbitrary waveform generator. The

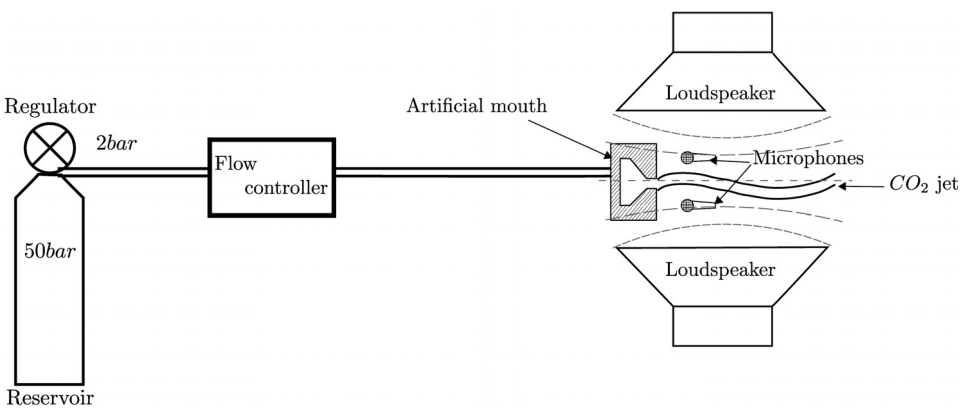

FIG. 9. Experimental setup.

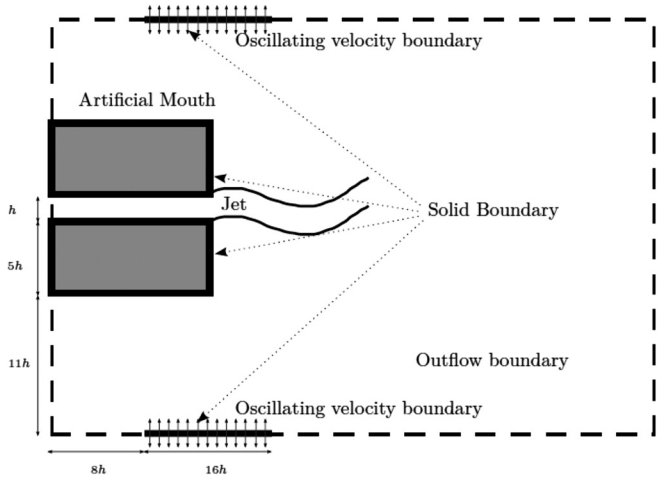

FIG. 10. Schematics of the simulation domain.

frequencies of the stroboscope and the acoustic excitation are tuned so that 50 different phases of the oscillation are visualized.

A camera including a fast shutter, set at 1 μs exposure time, is synchronized with the stroboscope. With this setup, we can reconstruct the jet oscillation by assembling images taken at different oscillation phases. This implies that the experiment is made in the permanent regime. A typical image of the experiments is shown in Fig. 2.

2. Numerical simulations setup

The goal of the simulations is to provide details of the flow in the vicinity of the flue. First, in order to fit the simulations with the experiment, the simulation domain is designed like the experimental setup, although some simplifications are needed. A Poiseuille flow in a channel separates at the flue, with the chosen geometry. The resulting jet is submitted to a transverse oscillating velocity. The simulations carried are two-dimensional and incompressible. In order to use the same post treatment as with the experiments, a numeric tracer is injected in the jet to visualize it: this is a non-physic quantity that is transported and diffused along the flow, used as an equivalent to smoke for visualization.

The following subsection discusses the tuning of the flow parameters with the aim of observing comparable jet behaviors and transverse disturbances in the simulations and the experiments. The behavior of the numerical configuration is then compared with theoretical results in a simple undisturbed jet spreading case.

a. Implementation of the simulation

A Poiseuille flow in a channel separates into a jet in the simulation domain. The domain is bounded by outflow conditions. To avoid vorticity reflection, the viscosity of the fluid is increased near the boundaries, in the direction tangential to the boundaries. Increasing the viscosity at the boundaries is a well-known technique used to attenuate vortices. Increasing the viscosity in the direction normal to the flow let the vortices damp without opposing to the flow exit. The viscosity of the fluid is taken into account by solving a diffusion equation for the velocity of the flow.

At the boundaries above and below the channel exit, a normal oscillating velocity is imposed with a no slip condition. The domain is represented on the Fig. 10, with the different lengths. Details of this setup has been described by Blanc *et al.*[13,20]

The simulations are carried using Gerris (Popinet[27,28]), an incompressible Navier-Stokes solver. The choice of an incompressible solver is motivated by the fact that the dimensions of the region considered and the velocities are small compared to the acoustic wavelengths λ and propagation velocity c_0 (i.e., $h \ll \lambda$ and $U_0 \ll c_0$).

All lengths of the domain are made dimensionless by the channel height h. Simulation parameters are tuned to match the experimental parameters, through Reynolds ($\mathrm{Re}=U_0 h/\nu$) and Strouhal ($St_h = \omega h/U_0$) numbers, two dimensionless numbers, where ν is the cinematic viscosity and U_0 the center velocity of the jet.

The viscosity is set so that $\mathrm{Re} = 375$ and the frequency of the disturbance is adjusted to produce a St_h between 0.1 and 0.9. The ratio between the acoustic disturbances v_{ac} and the center jet velocities U_0 at the channel exit are of the same order of magnitude in the simulations and the experimentations, that is $v_{ac}/U_0 = 0.025$ at a distance of $3\,h$.

It is noteworthy that due to mass conservation and the difference in lengths between the domain and the boundary where the oscillating velocity condition is set, one has to set the boundary oscillating velocity v_b greater than the velocity v_{ac} expected at the mouth level.

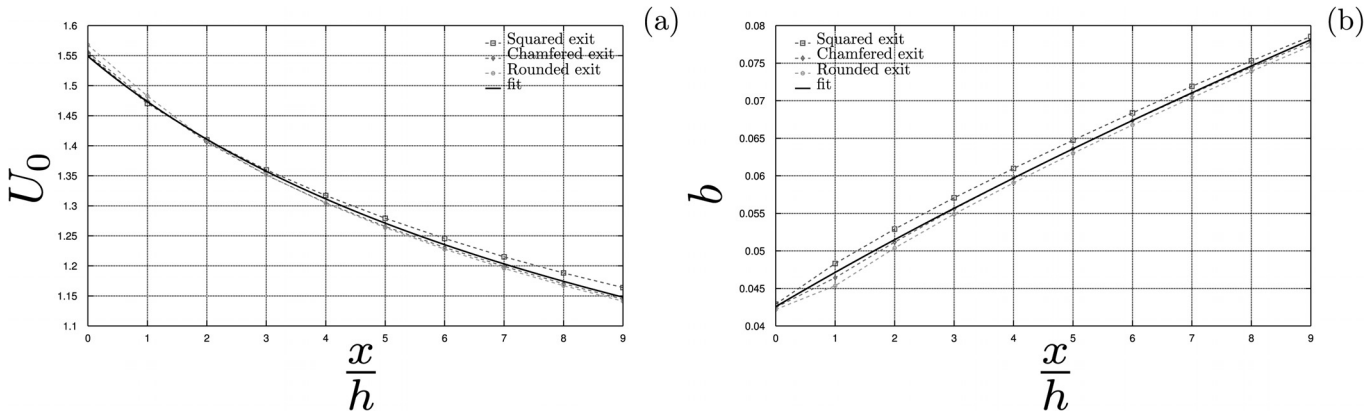

FIG. 11. Evolution of the parameters U_0 and b of the fitted Bickley profile versus the distance from the mouth.

Typically we set $v_b/U_0 = 0.1$ to obtain $v_{ac}/U_0 = 0.025$. As the oscillating boundaries are smaller, the disturbing field is less homogenous in the simulations than in the experiments, where the disturbances can be assumed to be of a constant amplitude all along the jet.

b. Jet spreading

The Gerris solver has been validated for test case problems[29] such as momentum conservation and Poiseuille flow convergence[30] and proves to be efficient in the incompressible Navier-Stokes computation. Fuster *et al.*[31] have also validated Gerris' ability to compute shear layer instabilities in the framework of the Orr−Sommerfeld description (Drazin[1]). In order to validate the numerical setup presented, an additional test, that suits better a jet configuration, is developed.

Simulations of free jets emerging from the geometries studied are carried out. Laminar viscous jets at long enough distance are known to adopt a Bickley velocity profile (Tritton[21]). Therefore the velocity profile of the free jet is expected to tend toward a Bickley profile far from the flue. After an arbitrary long time $t = 80(h/U_0)$, which is sufficiently long to assume that the flow is stationary, velocity profiles are taken at several distances from the channel exit. Those profiles are then fitted with a Bickley profile $U(y) = U_0 \mathrm{sech}^2\left(y - y^0/b\right)$.

Figure 11 shows the evolution of the central velocity and the parameter b of the fitted Bickley profile. They show that the evolution of the unperturbated jet does not depend on the geometry of the channel exit. A fit of the data shows the $x^{-1/3}$ evolution of the central velocity and the $x^{2/3}$ evolution of the width b, corresponding to the theoretical values for a Bickley jet (Tritton[21]). The velocity profile in the simulations evolves in agreement with the theory for laminar jets.

Figure 12 shows the mean quadratic error between the velocity profile and the fitted Bickley profile versus the distance from the mouth for the different exit geometries. This error is normalized by the central velocity of the fitted Bickley profile. The error decreases with distance, and reaches values below 0.5% at around $5\,h$. For distances greater than $7\,h$, not shown in the plot, the error raises because the laminar Bickley description becomes insufficient, as the jet begins to oscillate under the effect of its instrinsic instability. The depth of the chamfers for the chamfered exit and the radius of the rounded exit are both equal to $1h$. It is interesting to note that both error curves are shifted by approximately $1\,h$ to the right, relatively to the squared exit error curve. This means that despite the fact that the center velocities and width are comparable, the jet needs room to expand to a Bickley profile. Chamfers cause a delay to the Bickley profile dragging effect.

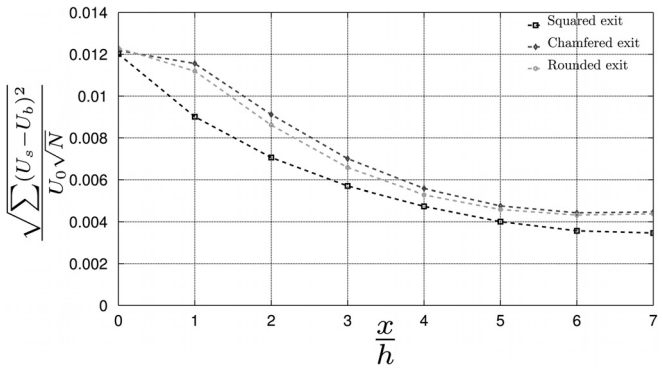

FIG. 12. Error between the velocity profile (U_s) and the fitted Bickley profile (U_b) normalized by the central velocity (U_0) versus the distance from the mouth.

[1]P. G. Drazin, *Introduction to Hydrodynamic Stability* (Cambridge University Press, Cambridge, UK, 2002), pp 160–178.
[2]J. W. S. Rayleigh, *The Theory of Sound* (Dover, New York, 1877), Vol. II, Chap, X. X.
[3]P. G. Drazin and L. N. Howard, "Hydrodynamic stability of parallel flow of inviscid fluid," Adv. Appl. Mechan. **9**, 1–89 (1966).
[4]M. Meissner, "Aerodynamically excited acoustic oscillations in cavity resonator exposed to an air jet," Acta Acust. Acust. **88**, 170–180 (2002).
[5]D. K. Holger, T. A. Wilson, and G. S. Beavers, "Fluid mechanics of the edgetone," J. Acoust. Soc. Am. **62**(5), 1116–1128 (1977).
[6]S. Dequand, J. F. H. Willems, M. Leroux, R. Vullings, M. van Weert, C. Thieulot, and A. Hirschberg, "Simplified models of flue instruments: Influence of mouth geometry on the sound source," J. Acoust. Soc. Am. **113**, 1724–1735 (2003).
[7]P. A. Nelson, N. A. Halliwell, and P. E. Doak, "Fluid dynamics of a flow excited resonance, Part II: Flow acoustic interaction," J. Sound Vib. **91**(3), 375–402 (1983).
[8]N. H. Fletcher, "Sound production by organ flue pipes," J. Acoust. Soc. Am. **60**(4), 926–936 (1976).
[9]M.-P. Verge, R. Caussé, B. Fabre, A. Hirschberg, A. P. J. Wijnands, and A. van Steenbergen, "Jet oscillations and jet drive in recorder-like instruments," Acta Acust. **2**, 403–419 (1994).
[10]C. Ségoufin, "Production de son par interaction écoulement/résonateur acoustique: Influence du système amont, application à la flûte à bec" ("Sound production by interaction between flow and acoustic resonance. Influence of upstream conditions, application to the recorder"), Ph.D. thesis, Université Pierre et Marie Curie, 2000.
[11]P. de la Cuadra, C. Vergez, and B. Fabre, "Visualization and analysis of jet oscillation under transverse acoustic perturbation," J. Flow Visualization Image Process. **14**, 355–374 (2007).
[12]C. Ségoufin, B. Fabre, M.-P. Verge, A. Hirschberg, and A. P. J. Winjnands, "Experimental study of the influence of the mouth geometry on sound production in a recorder-like instrument windway length and chamfers," Acta Acust. **86**, 649–661 (2000). Available at http://www.lam.jussieu.fr/Publications/Theses/ these-claire-segoufin.pdf.
[13]F. Blanc, "Production de son par couplage écoulement/résonateur: Étude des paramètres de facture des flûtes par expérimentations et simulations numériques d'écoulement" ("Sound production by flow/resonator coupling: An experimental and numerical study of sensitive flute making details)," Ph.D. thesis, Université Pierre et Marie Curie, Paris, France, 2009. Available at http://www.lam.jussieu.fr/Publications/Theses/these-francois-blanc.pdf.
[14]F. Blanc, P.-Y. Lagrée, B. Fabre, and A. Almeida, "Influence of the geometry of the channel exit on the jet birth in flue instruments," in *Proceedings of Isma 2007* (2007).
[15]N. H. Fletcher and S. Thwaites, "Wave propagation on an acoustically perturbed jet," Acustica **42**, 323–334 (1979).
[16]A. W. Nolle, "Sinuous instability of a planar jet: Propagation parameters and acoustic excitation," J. Acoust. Soc. Am. **103**(6), 3690–3705 (1998).
[17]G. E. Mattingly and W. O. Criminale, "Disturbance characteristics in a plane jet," Phys. Fluids **14**, 2258–2264 (1972).
[18]P. de la Cuadra, "The sound of oscillating air jets: Physics, modeling and simulation in flute-like instruments," Ph.D. thesis, University of Stanford, 2005. Available at http://www.lam.jussieu.fr/Publications/Theses/these-patricio-de-la-cuadra.pdf.
[19]M.-P. Verge, "Aeroacoustics of confined jets with applications to the physical modeling of recorder-like instruments," Ph.D. thesis, Technische Universiteit Eindhoven, 1995.
[20]F. Blanc, P.-Y. Lagrée, P. de la Cuadra, and B. Fabre, "Influence of the geometrical parameters in flue instruments on the vorticity modulation near the separation points of the jet," in *Proceedings of Acoustics'08* (2008).
[21]D. J. Tritton, *Physical Fluid Dynamics* (Oxford University Press, New York, 1999), Chap. 11, pp. 123–128.

[22]M.-P. Verge, B. Fabre, A. Hirschberg, and A. P. J. Wijnands, "Sound production in recorderlike instruments. I. Dimensionless amplitude of the internal acoustic field," J. Acoust. Soc. Am. **101**(5), 2914–2924 (1997).
[23]R. Auvray, B. Fabre, and P.-Y. Lagree, "Regime change and oscillation thresholds in recorder-like instruments," J. Acoust. Soc. Am. **131**(2), 1574–1585 (2012).
[24]See http://www.freefem.org/ (Last viewed 3/21/14).
[25]B. Fabre and A. Hirschberg, "Physical modeling of flue instruments: A review of lumped models," Acta Acust. Acust. **86**, 599–610 (2000).
[26]W. Merzkirch, *Flow Visualization* (Academic, London, 1987), pp. 134–139.
[27]S. Popinet, "Gerris: A tree-based adaptive solver for the incompressible Euler equations in complex geometries," J. Comput. Phys. **190**(2), 572–600 (2003). URL http://gfs.sf. net/gerris.pdf (Last viewed 3/21/14).
[28]S. Popinet, "Free computational fluid dynamics," ClusterWorld **2**(6), June 2004. URL http://gfs.sf.net/clusterworld/clusterworld.pdf (Date last viewed 3/21/14).
[29]See http://gfs.sourceforge.net/tests/tests/index.html (Last viewed 3/21/14).
[30]See http://gfs.sourceforge.net/tests/tests/poiseuille.html (Last viewed 3/21/14).
[31]D. Fuster, A. Bagué, T. Boeck, L. Le Moyne, A. Leboissetier, S. Popinet, P. Ray, R. Scardovelli, and S. Zaleski, "Simulation of primary atomization with an octree adaptive mesh refinement and VOF method," Int. J. Multiphase Flow **35**(6), 550–565 (2009).